THE JOURNAL OF BIOLOGICAL CHEMISTRY VOL. 281, NO. 38, pp. 27836–27845, September 22, 2006

Ligand Selectivity of Soluble Guanylyl Cyclase

*EFFECT OF THE HYDROGEN-BONDING TYROSINE IN THE DISTAL HEME POCKET ON BINDING OF OXYGEN, NITRIC OXIDE, AND CARBON MONOXIDE**

Received for publication, February 3, 2006, and in revised form, July 6, 2006 Published, JBC Papers in Press, July 24, 2006, DOI 10.1074/jbc.M601078200

Emil Martin[‡1], **Vladimir Berka**[§], **Elena Bogatenkova**[‡], **Ferid Murad**[‡2], **and Ah-Lim Tsai**[§3]

From the [‡]*Brown Foundation Institute of Molecular Medicine, University of Texas Health Science Center, and the* [§]*Department of Internal Medicine, Division of Hematology, University of Texas Houston Medical School, Houston, Texas 77030*

Although soluble guanylyl cyclase (sGC) functions in an environment in which O_2, NO, and CO are potential ligands for its heme moiety, the enzyme displays a high affinity for only its physiological ligand, NO, but has a limited affinity for CO and no affinity for O_2. Recent studies of a truncated version of the sGC β_1-subunit containing the heme-binding domain (Boon, E. M., Huang, S H., and Marletta, M. A. (2005) *Nat. Chem. Biol.*, 1, 53–59) showed that introduction of the hydrogen-bonding tyrosine into the distal heme pocket changes the ligand specificity of the heme moiety and results in an oxygen-binding sGC. The hypothesis that the absence of hydrogen-bonding residues in the distal heme pocket is sufficient to provide oxygen discrimination by sGC was put forward. We tested this hypothesis in a context of a complete sGC heterodimer containing both the intact α_1- and β_1-subunits. We found that the I145Y substitution in the full-length β-subunit of the sGC heterodimer did not produce an oxygen-binding enzyme. However, this substitution impeded the association of NO and destabilized the NO·heme complex. The tyrosine in the distal heme pocket also impeded both the binding and dissociation of the CO ligand. We propose that the mechanism of oxygen exclusion by sGC not only involves the lack of hydrogen bonding in the distal heme pocket, but also depends on structural elements from other domains of sGC.

Soluble guanylyl cyclase (sGC)[4] is a member of the guanylyl cyclase family of proteins, which respond to various ligands by converting GTP into cGMP. sGC stands apart from other members of its family by the nature of its activating ligand. Although other guanylyl cyclases are stimulated in response to various hormonal peptide ligands such as natriuretic peptides, guanylins, or toxins like heat-stable enterotoxin (see Ref. 1 for review), sGC is activated several hundredfold upon exposure to NO produced by nitric-oxide synthase. sGC is the key component of the NO/cGMP pathway and is crucial in mediating various physiological effects of NO such as blood vessel relaxation, inhibition of platelet aggregation, neurotransmission, and many others (2).

The affinity of the sGC enzyme for NO is mediated by the ferrous heme prosthetic group. sGC possesses a ligand selectivity unique for hemeproteins. NO binds to the sGC heme at rates that are almost diffusion-limited (3) to form a stable NO·heme complex. High affinity coupled with high specificity for NO is essential for sGC to function as an NO receptor. Although sGC functions in the intracellular environment containing 20–40 μM O_2 and up to 10 nM NO during NO synthesis (4), sGC is capable of discriminating between these two similar molecules in favor of NO. Moreover, even in the absence of NO, sGC does not form an oxyferrous heme complex and does not show any significant autoxidation. This is especially interesting considering that, in some aspects, the sGC heme is similar to the heme moiety of globin oxygen carriers such as myoglobins and hemoglobins. Similar to globins, the heme iron is in a 5-coordinate ferrous state with histidine as the proximal ligand. Until recently, the explanation for this oxygen exclusion by sGC included a weakened histidine–iron bond (5, 6) or a negative polarity in the surroundings of the sGC distal heme pocket (5). The absence of structural information hampered elucidation of this ligand selectivity.

Recently, several bacterial hemoproteins that share 15–40% sequence homology with the sGC heme domain have been identified. These proteins also have a proximal histidine ligand and contain a Y(S/R)T motif shown to interact with the propionic acid moiety of the sGC heme (7, 8). Analysis of the ligand specificity of several of these hemoproteins demonstrated that both NO and oxygen could be ligands for this group of proteins (9, 10). Thus, this group of proteins, which includes the β-subunit of mammalian sGC, was tentatively named H-NOX (heme-NO/oxygen binding (9)) or SONO (sensor of NO (11)). The x-ray structure of the heme sensor domain of an H-NOX protein from *Thermoanaerobacter tengcongensis* (11, 12) provided valuable information about the general fold of the heme-binding domain of the H-NOX family. Based on the x-ray structure of *T. tengcongensis* H-NOX, homology models of the sGC heme-binding pocket were predicted (9, 11, 12). None of these models show residues that would provide a negative polarity in the heme pocket of sGC. These analyses thus greatly disfavor the hypothesis of negative polarity in distal heme pocket (9).

* This work was supported in part by Grant 0465091Y from the American Heart Association, Texas Affiliate (to E. M.); by Grants HL64221 and GM61731 (to F. M.), Grant GM56818 (to A.-L. T.), and Subaward DK035153-17 (to E. M.) from the National Institutes of Health; and by the Dunn Foundation and the University of Texas (to F. M.). The costs of publication of this article were defrayed in part by the payment of page charges. This article must therefore be hereby marked "*advertisement*" in accordance with 18 U.S.C. Section 1734 solely to indicate this fact.

[1] To whom correspondence may be addressed. Tel.: 713-500-7567; Fax: 713-500-7455; E-mail: emil.martin@uth.tmc.edu.

[2] To whom correspondence may be addressed. Tel.: 713-500-7547; Fax: 713-500-0790; E-mail: ferid.murad@uth.tmc.edu.

[3] To whom correspondence may be addressed. Tel.: 713-500-6771; Fax: 713-500-6810; E-mail: ah-lim.tsai@uth.tmc.edu.

[4] The abbreviations used are: sGC, soluble guanylyl cyclase; TEA, triethanolamine; DEA-NO, 2-(*N*,*N*-diethylamino)diazenolate-2-oxide diethylammonium salt; PPIX, protoporphyrin IX.

The *T. tengcongensis* H-NOX structure also reveals that the distal heme pocket Tyr^{140}, which is conserved in H-NOX proteins from anaerobic bacteria (13), is crucial for ligand specificity. Under aerobic conditions, the *T. tengcongensis* H-NOX Tyr^{140} forms a hydrogen bond with a molecule of oxygen and stabilizes the heme·O_2 complex. It has been suggested that all H-NOX proteins with Tyr^{140} are oxygen sensors. However, in a heme sensor protein from *Clostridium botulinum*, this tyrosine does not form a hydrogen bond with oxygen, but stabilizes the complex with NO (11) even in the presence of oxygen. Thus, it appears that, despite a common protein fold of H-NOX proteins, slight differences in the structure may be crucial in determining the selectivity for gaseous ligands.

In the mammalian β-subunit of sGC, the ortholog position of this Tyr^{140} is Ile^{145}. The effect of the I145Y substitution in the heme domain of sGC on oxygen binding was tested in the fragment of the sGC β-subunit (residues 1–385) containing the heme-binding domain of the enzyme (10). Kinetic measurements of oxygen binding performed on the β_1-(1–385) I145Y mutant fragment as well as on the reverse substitution mutant (Y140I) of the *T. tengcongensis* H-NOX protein suggested that the distal pocket tyrosine is necessary and sufficient for oxygen binding in the H-NOX/SONO family of proteins. It has been proposed that lack of the distal tyrosine or of other hydrogen bond donors is the key determinant of the oxygen discrimination by the sGC enzyme (10, 13, 14).

As this conclusion was based on evidence derived from only a fragment of the sGC enzyme, we tested this hypothesis in the more natural context of the sGC heterodimer, which contains both the full-length α- and β-subunits. From previous reports, it also remained unclear how the tyrosine in the distal heme pocket of sGC affects the specificity of sGC protein for NO and CO. In this study, we present the catalytic and spectral properties of heterodimeric sGC carrying the I145Y substitution in the β-subunit. This mutation in full-length sGC significantly decreased the enzyme activation by NO, lowered the affinity for NO, and affected CO binding, but surprisingly did not facilitate oxygen binding under the tested conditions. On the basis of our data, we propose that the presence of hydrogen-bonding residues in the distal heme pocket is not sufficient to confer oxygen binding to the sGC heme and that contributions from other parts of the enzyme are critical in ligand discrimination. Moreover, introduction of a hydrogen-bonding tyrosine into the distal heme pocket strongly affects the binding characteristics of sGC for other gaseous ligands.

EXPERIMENTAL PROCEDURES

Protein Expression and Purification—Site-directed mutagenesis was used to generate the I145Y substitution in the coding region of the pVL-β baculoviral transfer vector (15). This vector was used to generate the baculovirus expressing the I145Y mutant sGC β-subunit (βI145Y). The wild-type and mutant sGC enzymes were expressed in Sf9 cells and purified as described previously (16). In short, a 100,000 × *g* supernatant was applied to a 30-ml DEAE FF-Superose column, and sGC-containing fractions were eluted with 350 mM NaCl and loaded onto a 20-ml nickel-agarose column with HisBind resin (Novagen). After a 50 mM imidazole wash, the sGC enzyme was eluted with 175 mM imidazole. To remove the imidazole, the sample was captured on a 5-ml HiTrap DEAE FF-Sepharose column (Amersham Biosciences), washed, and eluted with 300 mM NaCl. The sGC-containing fractions were concentrated on a Centricon YW-100 concentrator (Millipore). Preparations were at least 95% pure as determined by SDS-PAGE and by Coomassie Blue staining and immunoblotting as described previously (16). To prepare anaerobic samples, the enzyme sample was placed in a tonometer and subjected to five cycles of vacuum (30 s)/argon (5 min) replacement using an anaerobic train.

Assay of sGC Activity—Enzyme activity was assayed by formation of [^{32}P]cGMP from [α-^{32}P]GTP at 37 °C as described previously (17). Briefly, the reaction was initiated by addition of 1 mM GTP to the enzyme in 25 mM TEA (pH 7.5), 1 mg/ml bovine serum albumin, 1 mM 3-isobutyl-1-methylxanthine, 1 mM cGMP, 3 mM $MgCl_2$, 0.05 mg/ml creatine phosphokinase, and 5 mM creatine phosphate. Dilutions of 2-(*N*,*N*-diethylamino)diazenolate-2-oxide diethylammonium salt (DEA-NO) donor were prepared in 10 mM NaOH and added to the enzyme immediately before starting the reaction with GTP. The enzyme was incubated with GTP at 37 °C for 4 min, stopped by zinc acetate, and processed as described previously (17). To measure the extent of protoporphyrin IX (PPIX) activation, the Sf9 lysates containing wild-type or mutant enzyme were treated with 0.2% Tween 20 for 10 min on ice and then added to the reaction buffer containing various concentrations of PPIX. After a 10-min incubation, the reaction was initiated by addition of GTP. The activity of the CO-treated enzyme was measured in gas-tight vials using CO-equilibrated reaction buffers in the presence or absence of BAY41-2272 (5-cyclopropyl-2-[1-(2-fluorobenzyl)-1*H*-pyrazolo[3,4-*b*]pyridin-3-yl]-pyrimidin-4-ylamine). The allosteric regulator BAY 41-2272 was a generous gift from Bayer.

Time-resolved Measurement of NO·sGC Heme Complex Formation—Working NO solutions of different concentrations were prepared by transferring aliquots of a 1 mM NO stock solution into a gas-tight reaction syringe with N_2-saturated 50 mM TEA buffer (pH 7.4). The working solution was used immediately for time-resolved measurements.

Measurements of NO·sGC heme complex formation were conducted using a Bio-SEQUENTIAL DX-18MV stopped-flow instrument (Applied Photophysics Ltd., Leatherhead, UK) equipped with a rapid scan photodiode array detector and all fluid channels made of PEEK™ material. Before measurements, the stopped-flow apparatus was made anaerobic by filling the instrument for 2–5 h with anaerobic 0.1 M pyrophosphate buffer (pH 8.3) containing excess sodium dithionite. The anaerobic sGC solution was mixed with NO solutions at 24 °C in the stopped-flow instrument. Changes in the UV-visible spectra between 300 and 700 nm were recorded using the photodiode array detector at 400 scans/s.

To analyze the effect of GTP on the NO binding kinetics, a sequential mixing technique was applied. In the first mixing step, the enzyme was mixed with 5 mM GTP solution and incubated in an aging loop for 100 ms. In the second mixing step, the sample from the aging loop was mixed with NO solution, and changes in UV-visible spectra were recorded as described above.

To determine the binding rates of NO or CO ligands, changes at single wavelengths were monitored. The wavelengths used for the experiments were selected based on the analysis of the rapid scanning experiments. To determine the observed rate of ligand binding, the single wavelength traces were fitted to a single exponential function using built-in software. The observed rates were plotted *versus* the final concentrations of gaseous ligand in the reaction mixture. Plots for each analyzed ligand-enzyme pair were used to calculate k_{off}, k_{on}, and K_D as described later under "Results." Time-resolved measurements of CO·sGC complex formation were performed similarly, but under aerobic conditions with aerobic samples and buffers.

NO Titration Experiment—The anaerobic enzyme sample was prepared in a tonometer fitted with a cuvette and adaptor for a gas-tight syringe. A Hamilton syringe with a threaded plunger was used for this experiment. The volume delivered by each turn of the plunger was calibrated in advance. A saturated NO solution (1 mM) was prepared in 50 mM TEA buffer (pH 7.4) as described previously (16) and loaded into the syringe. The syringe adaptor was opened under continuous positive argon pressure, and the syringe with saturated NO solution was fitted into the adaptor. As a result, the head space of the assembled tonometer (~15 ml) was under positive argon pressure. NO was delivered directly into the enzyme solution by rotation of the calibrated screw at the end of the plunger. UV-visible spectra were recorded after each addition of NO on a Hewlett-Packard 8453 diode array spectrophotometer. Titration was continued until no further changes in the spectra were detected. We calibrated the effective amount of NO delivered under these experimental conditions by titrating oxyhemoglobin as an NO acceptor. Based on this calibration, it was determined that a 2-fold correction should be introduced to convert the amount of NO delivered by the syringe into the effective NO concentration dissolved in the sample. This discrepancy is due to positive argon pressure, which affects the solubility of NO.

EPR Measurement—The EPR samples of the NO·heme complex of sGC containing the I145Y mutant α- and β-subunits ($\alpha\beta$I145Y) were prepared by an anaerobic single turnover procedure as described previously (18). The protein sample was first subjected to vacuum/argon replacement cycles to make it anaerobic in a titration vessel with a glass magnetic bar to keep the enzyme solution under constant mixing. Anaerobic 50 μM NO solution was added via the rubber septum to the enzyme solution by an airtight syringe. After different incubation times (2–5 s) the positive argon pressure was applied to evacuate the reaction mixture via a stainless steel needle into an EPR tube flushed with argon. When ~3 cm of the EPR tube was filled with sample, the tube was immersed quickly in an acetone/dry ice bath to stop further reaction. The EPR tube was transferred to liquid nitrogen for storage and later EPR measurements. Western blotting was performed using rabbit anti-β- and anti-α-subunit polyclonal antibodies (Sigma) at 1:1000 dilution as primary antibodies, and the signal was visualized using ECL Plus detection reagent (GE Healthcare).

RESULTS

Catalytic Activity of $\alpha\beta$I145Y—To test the hypothesis that the absence of residues capable of forming hydrogen bonds dictates oxygen discrimination by sGC, we substituted Ile^{145} in the β-subunit with tyrosine. As a first step in the functional analysis of such a mutation, we coexpressed the I145Y mutant α- and β-subunits of human sGC ($\alpha\beta$I145Y) in Sf9 cells and tested the catalytic activity of the mutant enzyme. As demonstrated in Fig. 1, the mutant enzyme showed a decreased activation by 200 μM DEA-NO (10-fold *versus* 230-fold for the wild-type enzyme). Although the mutant was activated by the allosteric regulator BAY 41-2272, the enzyme was not responsive to stimulation by CO and showed a greatly reduced synergistic activation by a combination of CO and BAY 41-2272 (Fig. 1*A*). This is unlike the strong synergism of activation observed for the wild-type enzyme treated with CO and BAY 41-2272. It should be noted, however, that the mutation did not affect the stimulatory effect of manganese ion on the activity of the enzyme (Fig. 1*A*), suggesting that the function of the catalytic domain was not directly affected.

To analyze the effect of the mutation on the NO-dependent activation, we compared the DEA-NO activation response in the lysates containing the wild-type or $\alpha\beta$I145Y enzyme at different concentrations of the donor. The wild-type enzyme showed a strong activation with an EC_{50} of ~600 nM. However, the mutant enzyme, despite showing activation at all concentrations of DEA-NO, did not reach maximal activation even when 1 mM DEA-NO was applied (Fig. 1*B*). This behavior of the mutant enzyme suggests that the enzyme affinity for NO and/or enzyme activation was altered by the tyrosine.

To distinguish between these possibilities, we tested the effect of PPIX on the heme-depleted enzyme. PPIX effectively activates the enzyme in the absence of any gaseous ligands by replacing the ferrous heme moiety (19). Low concentrations of Tween 20 facilitates this replacement (17, 20) by promoting heme depletion. As demonstrated in Fig. 1*C*, the Sf9 lysate expressing the mutant enzyme showed a right shift in the PPIX activation response curve compared with the wild-type enzyme, possibly because of some steric hindrance induced by the tyrosine in the heme domain. In addition, we observed a decreased maximal activation of the mutant enzyme, which could not be explained by the difference in the expression levels (Fig. 1*C*, *inset*). It appears that introduction of a tyrosine into the heme domain interferes with propagation of the activating signal. This conclusion is corroborated by the absence of CO-dependent activation of the enzyme, by the lack of BAY 41-2272-induced synergism of CO activation, and by the significant right shift in the DEA-NO response curve. Thus, these data indicate that the perturbations in the heme-binding domain introduced by the I145Y substitution interfered with the activation process or the enzyme and may have affected the ligand affinity.

Spectral Properties of $\alpha\beta$I145Y—The UV-visible spectra of the purified $\alpha\beta$I145Y mutant displayed a Soret maximum at 430 nm and a broad α/β-band in the 560–590 nm range, which are identical to the wild-type enzyme spectral characteristics (21). Despite the presence of a tyrosine at position 145, we found no evidence of oxygen binding to the mutant in aerobic buffer (258 μM O_2) (Fig. 2*A*). The spectral properties did not change after oxygen was removed from the sample by several cycles of vacuum/argon replacement and remained the same

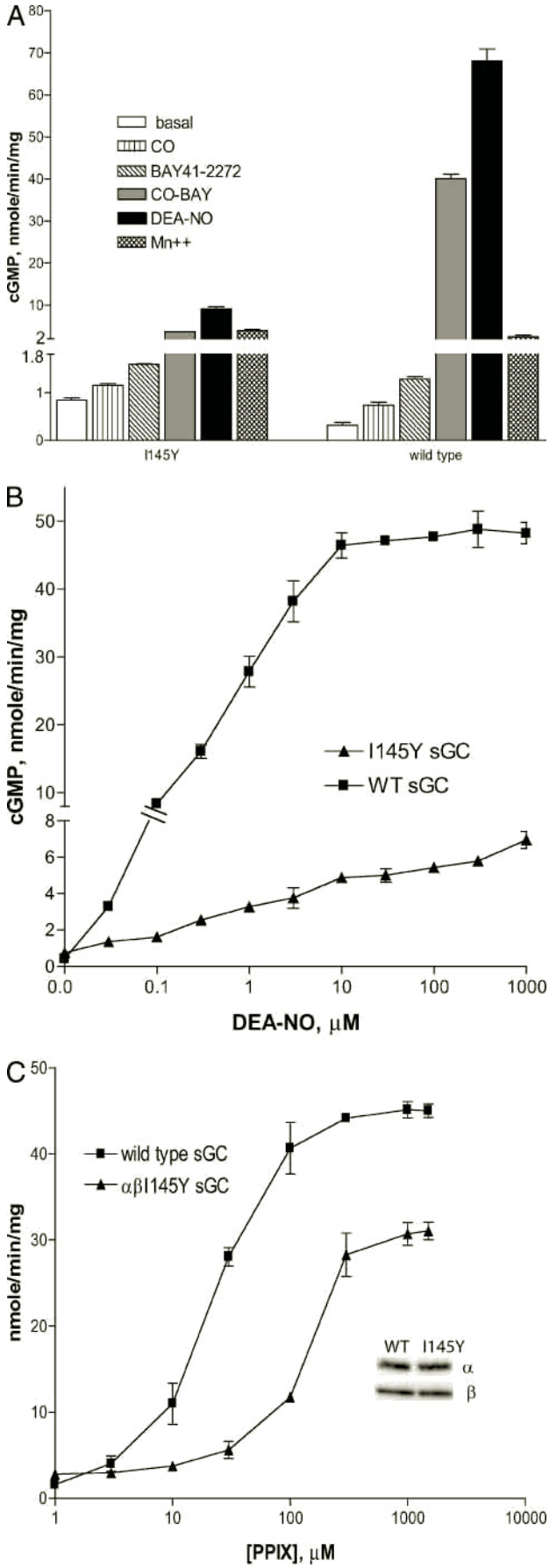

when placed under 1 atmosphere of O_2 (1.28 mM O_2) (Fig. 2*A*). Although no CO-dependent activation of the mutant was observed (Fig. 1), the exposure to CO shifted the Soret maximum to 423 nm and resulted in split α- and β-bands (Fig. 2*A*). This spectrum of the CO·$\alpha\beta$I145Y complex is identical to that of the CO·sGC (wild-type) complex (22) as shown in Fig. 2*B*. However, exposure of the mutant to NO resulted in a UV-visible spectrum different from that of the wild-type NO·sGC adduct. The NO·$\alpha\beta$I145Y complex showed a major Soret peak with a maximum at 417 nm and a shoulder at 399 nm, suggesting that the majority of NO·$\alpha\beta$I145Y is 6-coordinate (417 nm), whereas a smaller fraction of the complex becomes 5-coordinate. The ratio between the 417 and 399 nm bands did not change upon longer incubations (data not shown) or addition of a high concentration of DEA-NO (Fig. 2*A*).

To confirm the coordination structure of the NO·$\alpha\beta$I145Y complex, we recorded its EPR spectra. The spectrum of the EPR sample freeze-trapped after reaction of 10 μM $\alpha\beta$I145Y for 2–3 s with 5 eq of NO is shown in Fig. 2*C* (*upper trace*). This low spin NO·heme complex spectrum is fairly typical for a 6-coordinate NO·heme complex with a proximal imidazole ligand. Two sets of nitrogen hyperfine splitting were discernible: the ~22-G hyperfine splitting for the NO nitrogen (A_{NO}) and the ~8-G super-hyperfine splitting for the His^{105} imidazole nitrogen (A_{im}). The simulations for these EPR data (Fig. 2*C*, *middle trace*) indicate the positions of the three principal g values as 2.078 (g_x), 2.011 (g_z), and 1.986 (g_y) and anisotropic hyperfine splitting constants for both nitrogen nuclei as $A_{xx}/A_{yy}/A_{zz}$ = 17/16/31 for A_{NO} and $A_{xx}/A_{yy}/A_{zz}$ = 9/7/7 for A_{im}. When NO gas was replaced with 375 μM DEA-NO, the freeze-trapped NO·heme complex exhibited an EPR spectrum that was a mixture of both the 6- and 5-coordinate low spin heme complexes, with the former being the prominent species. The triplet hyperfine splitting of NO in the 5-coordinate complex (A_{NO} = 18.5 G) was superimposed upon a 6-coordinate NO·heme complex EPR spectrum with essentially identical structure as the *upper trace*.

Kinetics of NO Binding to αβI145Y—The different spectral characteristics of the mutant enzyme in complex with NO and the data from Fig. 1*B* clearly indicate that the nature of the

FIGURE 1. **Catalytic properties of αβI145Y.** *A*, comparison of sGC activity in Sf9 lysates expressing the wild-type and $\alpha\beta$I145Y mutant enzymes. The assay was performed either aerobically for treatment with 200 μM NO donor DEA-NO, 5 μM allosteric activator BAY 41-2272, or Mn^{2+} or anaerobically with CO-saturated buffers with or without 5 μM BAY 41-2272. To measure the extent of manganese stimulation, the reaction buffer contained 5 mM Mn^{2+} instead of 3 mM Mg^{2+}. The data of three independent measurements are presented as the means ± S.D. The specific activities of the untreated mutant and wild-type lysates were 0.84 ± 0.04 and 0.31 ± 0.05 nmol/min/mg, respectively. *B*, activation of purified wild-type (*WT*; ■) or $\alpha\beta$I145Y mutant (▲) sGC by various concentrations of DEA-NO. The data of three independent measurements are presented as the means ± S.D. The specific activities of the untreated mutant and wild-type enzymes were 0.6 ± 0.23 and 0.45 ± 0.18 nmol/min/mg, respectively. *C*, activation of the wild-type and mutant enzymes by PPIX. Lysates containing the same amount of the wild-type (■) or mutant (▲) enzyme were treated with 0.2% Tween 20 before incubation with reaction buffer containing various amounts of PPIX. The data of three independent measurements are presented as the means ± S.D. The specific activities of the untreated mutant and wild-type lysates were 0.72 ± 0.22 and 0.26 ± 0.07 nmol/min/mg, respectively. *Inset*, Western blotting of 10 μg of each lysate with anti-α- and anti-β-subunit antibodies indicated that the lysates expressed similar amounts of enzyme.

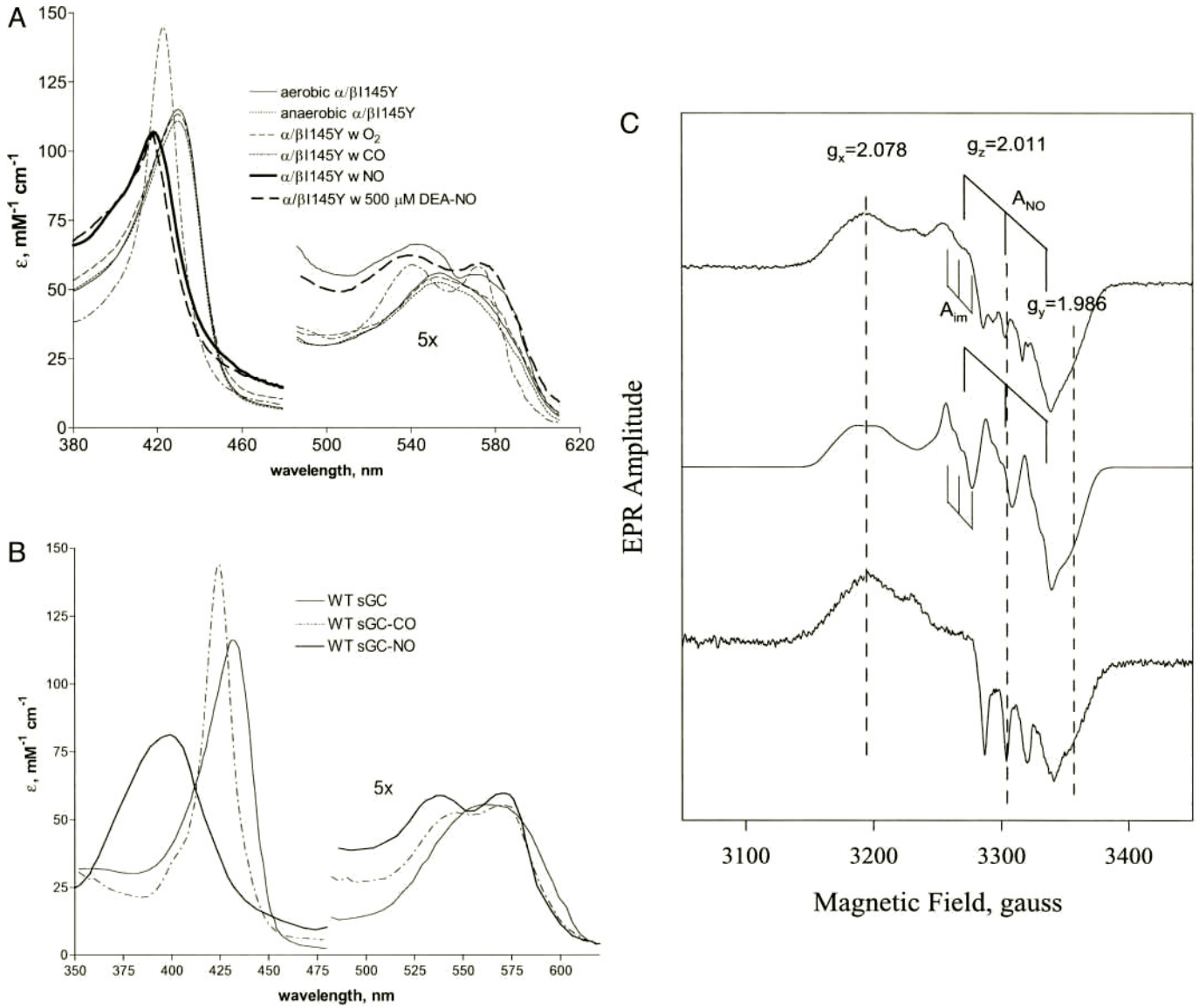

FIGURE 2. **Spectroscopic comparison of the wild-type and $\alpha\beta$I145Y mutant sGC enzymes exposed to O_2, CO, or NO.** *A*, the absorption spectra of the purified $\alpha\beta$I145Y enzyme in 50 mM TEA (pH 7.4) were recorded under the following conditions: aerobically (——), anaerobically (- - - -), under 1 atmospheric pressure of O_2 (– – –), under 1 atmospheric pressure of CO (– – -), and anaerobically after addition of NO solution to a final concentration of 20 μM (——) or 500 μM (— — —) DEA-NO. 3 μM $\alpha\beta$I145Y was used to record the NO mutant spectrum. *B*, the absorption spectra of the purified wild-type (*WT*) enzyme in 50 mM TEA (pH 7.4) were recorded under the following conditions: aerobically (——), under 1 atmospheric pressure of CO (– – -), and anaerobically after addition of NO solution to a final concentration of 40 μM (——). 4 μM sGC was used to record the NO·sGC spectrum. *C*, the EPR spectra of 10 μM $\alpha\beta$I145Y freeze-trapped are shown a few seconds after mixing with 50 μM NO solution (*upper trace*) or 5 min after addition of 375 μM DEA-NO (*lower trace*). The *middle trace* is the optimal stimulation for the *upper trace* using the parameters described under "Results." The EPR conditions were as follows: microwave frequency, 9.28 GHz; power, 4 milliwatts; modulation amplitude, 1 G; time constant, 0.33 s; and temperature, 116 K.

NO-sGC interaction is affected by introduction of a tyrosine into the heme domain. To determine the mechanism of such changes, we measured the NO binding kinetics of mutant sGC using the stopped-flow apparatus (Fig. 3). For comparison, the kinetics of NO binding to the wild-type enzyme is presented in Fig. 3*A*. In corroboration with previous reports (3, 16, 23), the binding of NO to the enzyme and the formation of the 6-coordinate intermediate were very fast and essentially completed in the dead time of the instrument, which agrees with the diffusion-limited rate of binding. This 6-coordinate intermediate was rapidly converted into the 5-coordinate NO·sGC complex (Fig. 3*A*). In several recent studies in which the kinetics of NO association was monitored after mixing the enzyme with NO donors, an apparent 6-coordinate intermediate was observed even after 12 and 16 s of measurements (24, 25). Moreover, it has been suggested that addition of GTP facilitates the transition from 6- to 5-coordinate NO·sGC complexes. Our measurements performed with predetermined concentrations of authentic NO (Fig. 3*A*) demonstrate that the 6-coordinate intermediate was clearly observed even in the presence of GTP (data not shown). Moreover, the rates of transition from 6- to 5-coordinate complexes estimated from the change in 420 nm absorbance (Fig. 3*A*, *inset*) were almost identical in the absence or presence of GTP: 17 and 14 s^{-1}, respectively. These data suggest that GTP had an insignificant effect on the NO binding step and thus allowed us to

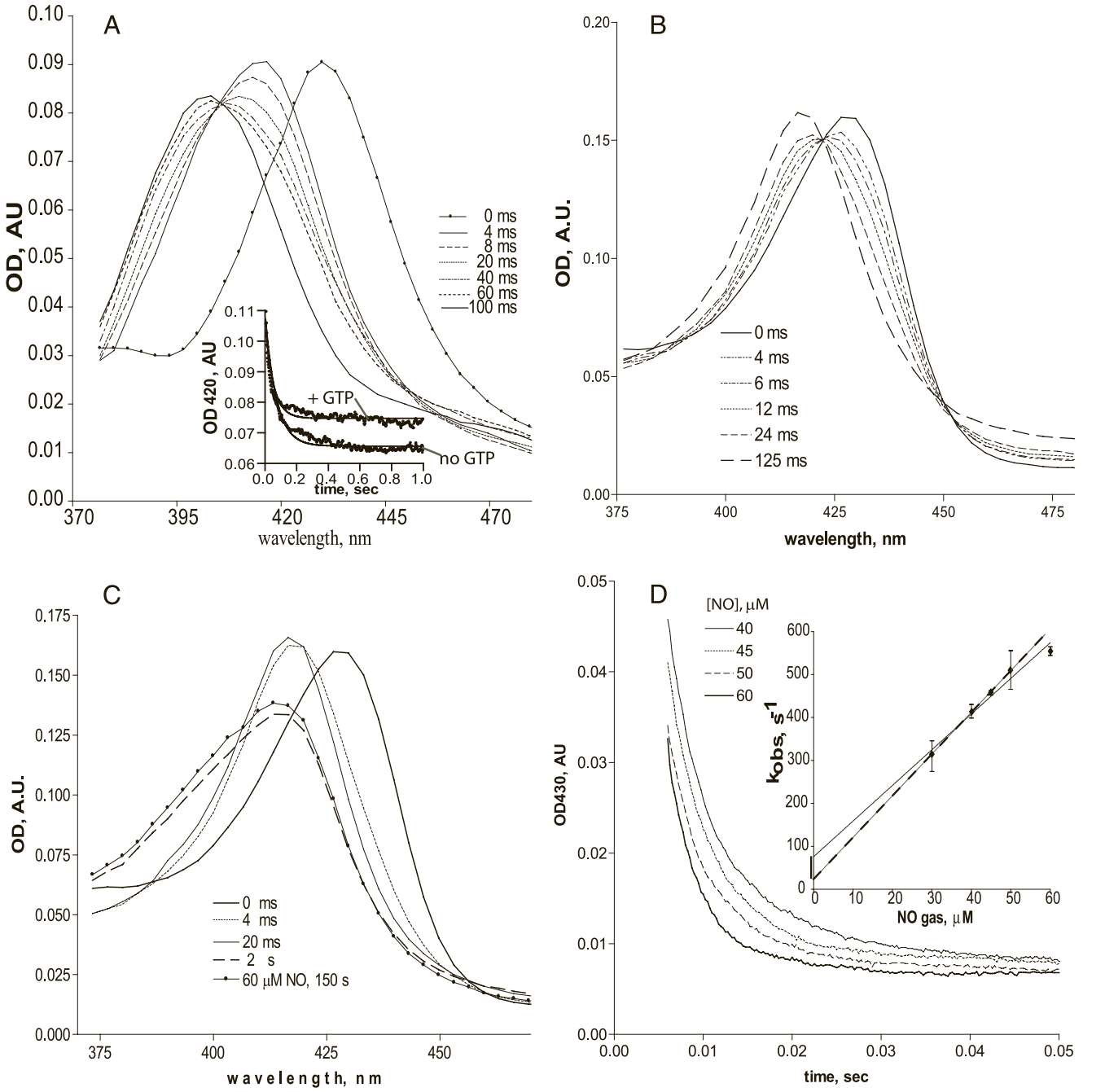

FIGURE 3. **Kinetic measurements of NO·$\alpha\beta$I145Y complex formation.** *A*, time-resolved changes in the spectra of 1.6 μM wild-type sGC after mixing with 2 μM NO. *Inset*, shown are the kinetics of the 420 nm changes in the presence and absence of GTP. *Dotted line*, experimental data; *solid line*, single exponential fit. *B* and *C*, time-resolved changes in the spectra of 1.5 μM $\alpha\beta$I145Y after mixing with equimolar NO or a 5-fold molar excess of NO, respectively. In all rapid scanning measurements, 400 spectra were collected in 1 s, and only several representative spectra are presented. *D*, kinetic data of changes in the 430 nm trace collected after mixing 4 μM $\alpha\beta$I145Y sGC with various concentrations of NO. Single exponential fits of the traces from the experiments satisfying pseudo first-order rate conditions were used to determine the observed rate (k_{obs}). At least three independent measurements for each concentration were performed. *Inset*, the plot of k_{obs} *versus* [NO] was used to determine k_{off} (ordinate intersection of linear regression), k_{on} (slope of linear regression), and K_D (k_{off}/k_{on}). *OD*, optical density; *AU*, absorbance units.

monitor the kinetics of NO binding to the mutant enzyme in the absence of GTP.

To ensure that the time-resolved changes in the spectra of the mutant can be monitored, we first used low concentrations of NO. Rapid scan stopped-flow measurements performed with stoichiometric amounts of ligand showed that NO binding caused an almost complete shift from the 430 nm Soret maximum to 417 nm with an isosbestic point at 423 nm (Fig. 3*B*), suggesting a single step transition to a 6-coordinate complex. Such a transition has not been previously recorded with the wild-type enzyme because of the very fast kinetics of NO binding. Increasing amounts of NO (5-fold molar excess) not only accelerated the formation of the 6-coordinate nitrosyl heme, but also resulted in a partial transition of the NO·heme complex into a 5-coordinate state (Fig. 3*C*). However, the proportion of the 5-coordinate nitrosyl heme did not increase even when the

TABLE 1

Ligand specificities for wild-type sGC, the αβI145Y mutant, and the model heme compound

NA, not applicable; 1-MeIm, 1-methylimidazole.

	K_D	k_{off}	k_{on}	Ref.
	M	s^{-1}	$M^{-1}\,s^{-1}$	
Wild-type sGC				
CO	2.6×10^{-4}	10.7	4×10^{4}	This study
NO	4.2×10^{-12} [a]	6×10^{-4}	1.4×10^{8}	3, 40, 41
O_2	NA	NA	NA	
αβI145Y sGC				
CO	2.5×10^{-4}	0.8	3×10^{3}	This study
NO	$1.2–9.1 \times 10^{-6}$	12–76	$8.3–9.9 \times 10^{6}$	This study
O_2	NA	NA	NA	This study
Fe(II)·PP·1-MeIm				
CO	1.3×10^{-9}	2.3×10^{-3}	1.8×10^{6}	42
NO	1.6×10^{-12}	2.9×10^{-4}	1.8×10^{8}	42
O_2	0.6×10^{-5}	3×10	5.5×10^{7}	43

[a] Calculated as k_{off}/k_{on} using values from Refs. 3 and 40.

concentration of NO was quadrupled (Fig. 3*C*, *60 μM NO trace*) and the incubation time was increased to 150 s, suggesting that the reaction was complete and this is the final state of the NO·αβI145Y complex. This property of the αβI145Y mutant contrasts with the NO binding feature of the wild-type enzyme (Fig. 3*A*), which bound NO very fast and formed a 5-coordinate NO·heme complex.

To calculate the rates of NO binding to αβI145Y, time-resolved changes in the 430 nm kinetics were recorded at different NO concentrations. All traces were fit to a single exponential function (Fig. 3*D*) to obtain the observed NO binding rates (k_{obs}) for each NO concentration. Plotting k_{obs} as a function of NO concentration allows the determination of the NO association rate constant (k_{on}) as the slope of the graph and of the NO dissociation rate constant (k_{off}) as the *y* axis intercept. The data point collected at 60 μM NO displayed an observed rate of 550 s^{-1}, indicating that >60% of the reaction was lost in the dead time of the instrument and that the value itself may be inaccurate. By ejecting this point, $k_{on} = 9.9 \times 10^{6}\ M^{-1}\ s^{-1}$, $k_{off} = 12\ s^{-1}$, and thus $K_D = 1.2$ μM were obtained (Table 1). If the point was retained, $k_{on} = 8.3 \times 10^{6}\ M^{-1}\ s^{-1}$, $k_{off} = 76\ s^{-1}$, and $K_D = 9$ μM were estimated (Table 1). Both the 9 and 1.2 μM estimations for the K_D value indicate that introduction of the tyrosine into the heme pocket significantly lowered the affinity for NO compared with the wild-type enzyme, which has a picomolar K_D for NO (Table 1). This decreased affinity is due to both decreased NO association and increased NO dissociation rate constants.

To determine which of the estimations is more accurate, we titrated an anaerobic sample of the αβI145Y enzyme with increasing amounts of saturated NO solution as described under "Experimental Procedures." If the K_D is 9 μM, a hyperbolic binding curve is expected in the 2–40 μM range of NO concentration. If, however, the K_D is 1 μM or less, we should expect a linear titration plot with a clear break when the plateau is reached. Changes in the UV-visible spectra of the sample were recorded after each addition of NO solution (Fig. 4*A*) and plotted as concentration of the NO·enzyme complex *versus* the effective NO concentration (Fig. 4*B*). A 7 μM stoichiometry for sGC estimated from a well defined break point of the plot (Fig. 4*B*, *vertical line*) is in good agreement with the 5.5 μM concentration of the enzyme used in the experiment. This outcome gave strong support for a K_D of 1.2 μM or less rather than 9 μM.

Kinetics of CO Binding to αβI145Y—Because introduction of the tyrosine into the heme pocket decreased the affinity for NO by decreasing the NO binding rate and destabilized the NO·heme complex, we tested the characteristics of CO binding as well. We measured the kinetics of CO binding to the wild-type and mutant enzymes by following the changes in 420 nm absorbance after mixing with various concentrations of CO (Fig. 5). We found that, although both wild-type sGC and the αβI145Y mutant displayed similar dissociation constants (K_D) of 260 and 250 μM, respectively, there was a significant kinetic difference in CO binding to these enzymes. The mutant enzyme showed a 10-fold decrease in both k_{on} and k_{off} compared with the wild-type enzyme (Table 1). These data indicate that, similar to NO binding, introduction of Tyr^{145} slowed CO binding; but, unlike the NO·heme complex, the k_{off} of the CO·heme complex was decreased 10-fold by the mutation.

DISCUSSION

Ligand Selectivity—Although, in the intracellular milieu, O_2, CO, and NO are potential ligands for various hemeproteins, sGC displays a high affinity for its physiological ligand (NO), only a limited affinity for CO, and no affinity for oxygen. Table 1 lists the dissociation constants for these three ligands determined for a water-soluble model heme compound, Fe(II)·PP·1-methylimidazole. Similar to the heme moiety of sGC, Fe(II)·PP·1-methylimidazole has a 5-coordinate ferrous iron with imidazole as the proximal ligand. As evident from the comparison, sGC displayed an affinity for the NO ligand remarkably similar to the model compound (Table 1). However, sGC bound CO with an affinity at least 2 orders of magnitude lower and showed no binding of O_2 (Table 1). This comparison implies that sGC protein creates a heme environment in which NO binding is not impeded, whereas both O_2 and CO are strongly excluded as ligands. Because cells produce only a limited amount of CO through heme oxygenase enzymes, the exclusion of CO does not have to be as rigorous as that of oxygen.

Mechanism of Oxygen Exclusion—In this study, we tested the hypothesis that the absence of hydrogen-bonding residues in the distal heme pocket confers the exclusion of O_2 by sGC. We

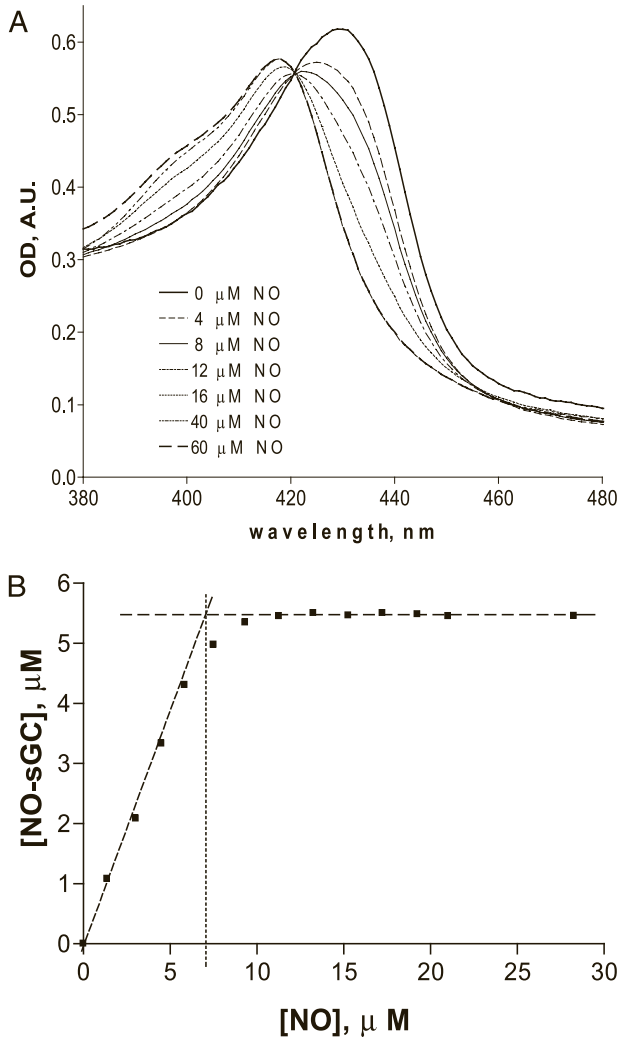

FIGURE 4. **Estimation of $\alpha\beta$I145Y mutant K_D for NO by NO gas titration.** *A*, changes in the absorption spectra of 5 μM $\alpha\beta$I145Y mutant during titration with NO solution. NO concentrations correspond to the added amount of NO. *B*, NO titration curves plotted as the concentration of the NO·$\alpha\beta$I145Y complex (5- plus 6-coordinate) *versus* the effective concentration of NO. A conversion coefficient was used to calculate the effective concentration of NO as described under "Experimental Procedures." *OD*, optical density; *AU*, absorbance units.

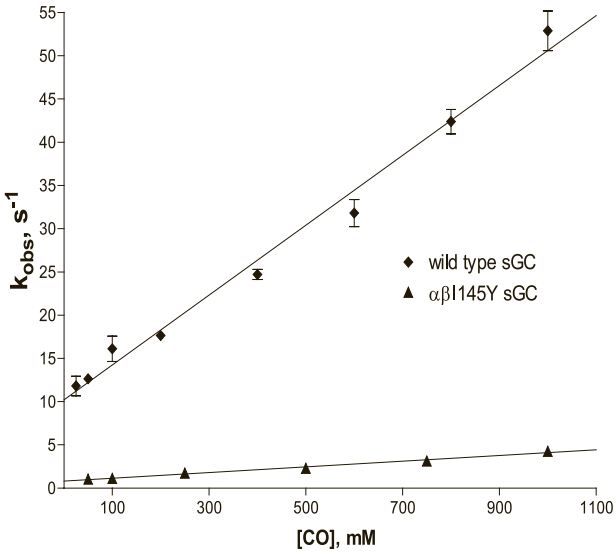

FIGURE 5. **Comparison of the CO binding characteristics of the wild-type and $\alpha\beta$I145Y sGC enzymes.** Transient absorption spectra at 420 nm were collected after mixing 2 μM wild-type or $\alpha\beta$I145Y sGC with various concentrations of CO (25–1000 μM). The k_{obs} values determined were plotted *versus* CO concentration, and the k_{off}, k_{on}, and K_D values were calculated.

analyzed the effect of the I145Y substitution in intact sGC containing both the α- and β-subunits. We found no evidence of oxygen binding even at 1.28 mM O_2. Previous kinetic measurements of oxygen binding performed on a β_1-(1–385) I145Y mutant fragment (10) and on the reverse substitution mutant (Y140I) of the *T. tengcongensis* H-NOX protein (10) suggested that the distal pocket tyrosine is necessary and sufficient for oxygen binding in the H-NOX/SONO family of proteins. It should be noted that the K_D of 70 mM for O_2 calculated from the measurement of oxygen binding to β_1-(1–385) I145Y (10) is at odds with experimental data from the same report. Spectral data indicate that the K_D for O_2 is closer to 2×10^{-4} M because the β_1-(1–385) I145Y protein binds oxygen in aerobic buffer (~258 μM O_2), albeit with rather slow kinetics (10). Even with this correction, the affinity of β_1-(1–385) I145Y for oxygen is at least an order of magnitude lower than that of the Fe(II)·PP·1-methylimidazole model heme compound ($K_D \sim 0.6 \times 10^{-5}$ M) (Table 1). This implies that, even in the presence of the hydrogen-bonding tyrosine in the distal heme pocket, the enzyme is still discriminating against oxygen. This discrepancy in oxygen binding properties between $\alpha\beta$I145Y and β_1-(1–385) I145Y indicates that the absence of hydrogen-bonding residues in the distal heme pocket is not sufficient to explain the exclusion of oxygen as a heme ligand for sGC. Moreover, the heme sensor protein from *C. botulinum*, which has high homology to *T. tengcongensis* H-NOX protein and carries tyrosine at the ortholog position (Ile^{145}), also does not bind oxygen, but has a femtomolar K_D for NO (11). Structural determinants in other domains of the β- and/or α-subunit appear to be necessary for the ligand selectivity of sGC. Although the β_1-(1–385) heme domain was shown to be an excellent model for investigating NO binding to sGC (3, 26, 27), analysis of this domain alone is not sufficient to elucidate the mechanism of oxygen exclusion by sGC. Detailed structure-function studies that take into consideration the contribution of both subunits may allow identification of the determinants responsible for the ligand selectivity. Although we did not observe any oxygen binding, introduction of Tyr^{145} into the distal heme pocket of the $\alpha\beta$-enzyme affected the binding of NO and CO.

Effects of the Distal Pocket Tyrosine on CO Binding—The tyrosine in the distal heme pocket of sGC affected the interaction of heme and CO. The kinetics of CO binding showed that the k_{on} for CO decreased. Our data corroborate the report on the *T. tengcongensis* H-NOX Y140L mutant enzyme (10), which displays a higher geminate rebinding of CO compared with native *T. tengcongensis* H-NOX. This change in the CO k_{on} reflects the steric conflict between the linear geometric requirement of the Fe–CO bond and the bulky phenyl ring of Tyr^{145} (Fig. 6). Interestingly, once bound, the CO molecule has to overcome the same steric hindrance by the Tyr^{145} side chain to dissociate, as evident from the decreased k_{off} (Table 1) of the CO·heme complex of $\alpha\beta$I145Y. Similar parallel changes in both association and dissociation rate constants for cyanide binding to ferric

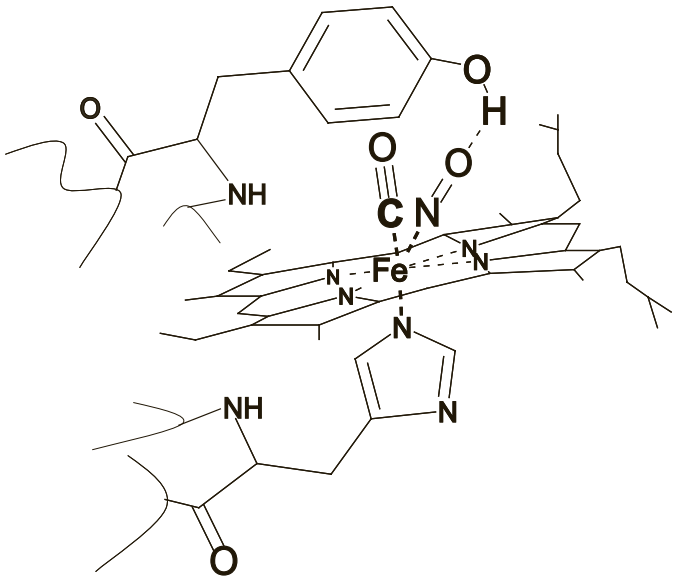

FIGURE 6. **Schematic representation of the possible effect of Tyr^{145} on CO and NO binding to $\alpha\beta$I145Y.** CO binds axially to the heme iron. The phenyl ring of the tyrosine impedes both the binding of CO (lower k_{on}) and the dissociation of CO molecules already bound (lower k_{off}). NO binds to the heme moiety in a bent mode. Hydrogen bonding by the phenol group of the tyrosine hampers the NO association (lower k_{on}), whereas the same hydrogen bonding also reduces Fe–NO bond strength, facilitating the release of the NO molecule (higher k_{off}).

endothelial nitric-oxide synthase in response to the binding of L-Arg substrate have been described previously (28).

Effects of the Distal Pocket Tyrosine on NO Binding—As in the case of CO binding, Tyr^{145} clearly impedes the access of NO to the heme moiety, as demonstrated by a significant decrease in the NO association rate constant (k_{on}) in comparison with wild-type sGC (Table 1). In contrast to CO, the NO k_{off} was higher by several orders, reflecting the destabilization of the NO·heme complex by the tyrosine (Table 1). We propose that such destabilization occurs owing to hydrogen bonding of NO with the hydroxyl group of Tyr^{145} (Fig. 6), leading to weaker Fe–NO ligation. Unlike the linear geometry of the Fe–CO bond, the Fe–NO bond is mostly nonlinear (29). Such nonlinear bonding may facilitate the formation of the hydrogen bond with the hydroxyl group. However, this hydrogen bond between Tyr^{145} and NO is not optimal and thus strains the Fe–NO bond and reduces the bond strength. This combination of reduced k_{on} and increased k_{off} led to a decreased K_D of NO for $\alpha\beta$I145Y to a micromolar range (Table 1), therefore allowing, for the first time, the recording of the binding kinetics of 6-coordinate NO·sGC complex formation (Fig. 4*A*). The presence of a well defined isosbestic point at 423 nm indicates that this conversion from 5-coordinate sGC to 6-coordinate NO·sGC is a single step process.

Introduction of the tyrosine not only affected the kinetics of NO binding, but also changed the coordination state of the formed NO·heme complex. As proven by absorbance and EPR spectra, the majority of the formed NO·heme complex is 6-coordinate (Fig. 2). It is proposed that, in the case of wild-type sGC, the electron transfer from NO to the heme iron leads to a repulsive *trans*-effect on the proximal His^{105}, resulting in cleavage of histidine–iron coordination (30, 31). However, introduction of the tyrosine into the $\alpha\beta$I145Y enzyme reduced this "*trans*-effect" as evidenced by a stable 6-coordinate NO·heme complex. We propose that the phenol ring of Tyr^{145} is capable of withdrawing some of the NO electron density away from the heme iron, resulting in an elongated Fe–NO bond. Such nonoptimal hydrogen bonding decreases the *trans*-effect and prevents the scission of the coordinating bond with His^{105}. The mixture of 5- and 6-coordinate NO·heme complexes found in $\alpha\beta$I145Y was also recently observed for the H-NOX proteins from *Legionella pneumophila* and *Nostoc punctiforme* (32). In these proteins, the mixture was converted into the 5-coordinate complex after increasing the temperature. Such a feature is similar to the *T. tengcongensis* H-NOX/SONO protein, which is 6-coordinate at 25 °C (9, 11) and 5-coordinate at 70 °C (11). Such a change in coordination suggests that a slight conformational difference due to either a temperature change or a different protein environment displaces the tyrosine in relation to the heme and heme iron, resulting in a protein with different properties. The effect of a different protein environment is well exemplified by the difference between $\alpha\beta$I145Y and *C. botulinum* SONO, which has a 19% sequence similarity to sGC. Both proteins contain a tyrosine in the ortholog position (βIle^{145}) and bind NO. However, *C. botulinum* SONO has a femtomolar affinity for NO (11), whereas $\alpha\beta$I145Y only a micromolar affinity. A slightly different placement of the tyrosine in *C. botulinum* SONO apparently disfavors the formation of the hydrogen bond with NO, resulting in a much more stable NO·heme complex. Interaction of tyrosine with other amino acid side chains at the distal heme pocket probably contributes to such a drastic difference in ligand specificity. Similar affinity-changing interactions have been characterized for the Tyr-Glu pair in the distal heme pocket of globins (33, 34) and the Tyr-Thr pair in the minihemoglobin of the nemertean worm *Cerebratulus lacteus* (35).

Future studies (such as x-ray crystallography and resonance Raman spectroscopy) of the NO·$\alpha\beta$I145Y and CO·$\alpha\beta$I145Y complexes may provide a more detailed explanation of the effect of the distal tyrosine on the specificity for different ligands. Careful comparison of the resonance Raman spectra of the β-(1–385) and β_1-(1–385) I145Y fragments with the spectra of the $\alpha\beta$-enzyme and $\alpha\beta$I145Y may also provide insights into the validity of the hypothesis of oxygen discrimination due to a weaker histidine–iron bond.

It should be noted that, except for this study, all previously reported spectral properties of the H-NOX family members were obtained only with the stand-alone heme sensor domains. Some of the H-NOX proteins, including *T. tengcongensis* H-NOX, are part of the larger protein, whereas others may be in complex with other proteins, *e.g.* histidine kinase, as part of the two-component system of gaseous sensors (13). Comparison of the oxygen binding properties of the β_1-(1–385) I145Y fragment and the complete $\alpha\beta$I145Y heterodimer suggests that the heme sensor domains may have, in their physiological environment, ligand specificity different from the specificity of the stand-alone domains.

Measurements of $\alpha\beta$I145Y mutant activity also highlight a previously overlooked gap between the NO binding step and sGC activation process. The $\alpha\beta$I145Y enzyme did not reach full

activation at millimolar concentrations of DEA-NO (Fig. 1*B*), although micromolar NO concentrations were sufficient to form an NO·heme complex (Figs. 2*A* and 4*B*). Similarly, wild-type sGC bound NO with a picomolar K_D (Table 1), but catalytic activation was observed only at high nanomolar concentrations of NO, judging from the dose-response plot from Fig. 1*B* and numerous similar plots published previously (36–38). Activation of the wild-type enzyme with low nanomolar concentrations of NO donors can be achieved by treatment with allosteric activators (36, 38), indicating that the NO·sGC complex is formed, but not fully active. This large concentration gap between NO binding and NO-dependent activation for both the mutant and wild-type enzymes indicates that NO binding is not the rate-limiting step in sGC activation. Subsequent events, which may also be NO-dependent (25, 39), dictate the rate of enzyme activation. Although it is rather challenging to investigate the activation process of wild-type sGC operating with nanomolar or even picomolar concentrations of NO because of its instability, the mutant appears to be a new useful tool of investigation. Decreased affinity for activating ligand and the subsequent signal transduction bring the activation process into a comfortable range of NO concentrations for future investigations into the complex mechanism of sGC activation.

In summary, our data indicate that introduction of the hydrogen-bonding tyrosine into the distal region of the heme pocket of a full-length sGC heterodimer caused distinctive effects on O_2, NO, and CO ligand binding. No oxygen binding was observed. We therefore propose that the mechanism of oxygen exclusion by sGC not only involves the lack of hydrogen bonding in the distal heme pocket, but also depends on structural elements from other domains of sGC. However, a substantial decrease in NO affinity was observed. We propose that non-optimal hydrogen bonding with tyrosine significantly reduces the association of the NO ligand and also enhances the dissociation of the NO·heme complex. Although CO affinity was little changed, a large decrease in both the association and dissociation rate constants was observed. We believe that this is the consequence of the steric hindrance by the tyrosine phenyl ring on the CO ligand. Introduction of a tyrosine into the heme pocket also affected the enzyme activation process, induced by NO binding. Thus, in comparison with the model heme system, it appears that tyrosine was evolutionary excluded from the heme pocket of sGC not to prevent oxygen binding, as proposed previously (13, 14), but to avoid steric hindrance and to ensure optimal binding of NO to the heme and subsequent enzyme activation.

REFERENCES

1. Lucas, K. A., Pitari, G. M., Kazerounian, S., Ruiz-Stewart, I., Park, J., Schulz, S., Chepenik, K. P., and Waldman, S. A. (2000) *Pharmacol. Rev.* **52,** 375–414
2. Martin, E., Sharina, I., Seminara, A. R., Krumenacker, J., and Murad, F. (2005) in *Nitric Oxide, Cell Signaling and Gene Expression* (Lamas, S., and Cadenas, E., eds) pp. 167–216, Taylor & Francis Group, Boca Raton, FL
3. Zhao, Y., Brandish, P. E., Ballou, D. P., and Marletta, M. A. (1999) *Proc. Natl. Acad. Sci. U. S. A.* **96,** 14753–14758
4. Condorelli, P., and George, S. C. (2001) *Biophys. J.* **80,** 2110–2119
5. Deinum, G., Stone, J. R., Babcock, G. T., and Marletta, M. A. (1996) *Biochemistry* **35,** 1540–1547
6. Oertling, W. A., Kean, R. T., Wever, R., and Babcock, G. T. (1990) *Inorg. Chem.* **29,** 2633–2645
7. Schmidt, P. M., Rothkegel, C., Wunder, F., Schroder, H., and Stasch, J. P. (2005) *Eur. J. Pharmacol.* **513,** 67–74
8. Schmidt, P. M., Schramm, M., Schroder, H., Wunder, F., and Stasch, J. P. (2004) *J. Biol. Chem.* **279,** 3025–3032
9. Karow, D. S., Pan, D., Tran, R., Pellicena, P., Presley, A., Mathies, R. A., and Marletta, M. A. (2004) *Biochemistry* **43,** 10203–10211
10. Boon, E. M., Huang, S. H., and Marletta, M. A. (2005) *Nat. Chem. Biol.* **1,** 53–59
11. Nioche, P., Berka, V., Vipond, J., Minton, N., Tsai, A.-L., and Raman, C. S. (2004) *Science* **306,** 1550–1553
12. Pellicena, P., Karow, D. S., Boon, E. M., Marletta, M. A., and Kuriyan, J. (2004) *Proc. Natl. Acad. Sci. U. S. A.* **101,** 12854–12859
13. Boon, E. M., and Marletta, M. A. (2005) *J. Inorg. Biochem.* **99,** 892–902
14. Boon, E. M., and Marletta, M. A. (2005) *Curr. Opin. Chem. Biol.* **9,** 441–446
15. Lee, Y. C., Martin, E., and Murad, F. (2000) *Proc. Natl. Acad. Sci. U. S. A.* **97,** 10763–10768
16. Martin, E., Berka, V., Tsai, A.-L., and Murad, F. (2005) *Methods Enzymol.* **396,** 478–492
17. Martin, E., Sharina, I., Kots, A., and Murad, F. (2003) *Proc. Natl. Acad. Sci. U. S. A.* **100,** 9208–9213
18. Tsai, A.-L., Kulmacz, R. J., and Palmer, G. (1995) *J. Biol. Chem.* **270,** 10503–10508
19. Ignarro, L. J., Wood, K. S., and Wolin, M. S. (1982) *Proc. Natl. Acad. Sci. U. S. A.* **79,** 2870–2873
20. Foerster, J., Harteneck, C., Malkewitz, J., Schultz, G., and Koesling, D. (1996) *Eur. J. Biochem.* **240,** 380–386
21. Gerzer, R., Bohme, E., Hofmann, F., and Schultz, G. (1981) *FEBS Lett.* **132,** 71–74
22. Stone, J. R., and Marletta, M. A. (1994) *Biochemistry* **33,** 5636–5640
23. Makino, R., Matsuda, H., Obayashi, E., Shiro, Y., Iizuka, T., and Hori, H. (1999) *J. Biol. Chem.* **274,** 7714–7723
24. Russwurm, M., and Koesling, D. (2004) *EMBO J.* **23,** 4443–4450
25. Cary, S. P., Winger, J. A., and Marletta, M. A. (2005) *Proc. Natl. Acad. Sci. U. S. A.* **102,** 13064–13069
26. Zhao, Y., Schelvis, J. P., Babcock, G. T., and Marletta, M. A. (1998) *Biochemistry* **37,** 4502–4509
27. Schelvis, J. P., Zhao, Y., Marletta, M. A., and Babcock, G. T. (1998) *Biochemistry* **37,** 16289–16297
28. Berka, V., Chen, P.-F., and Tsai, A.-L. (1996) *J. Biol. Chem.* **271,** 33293–33300
29. McCleverty, J. A. (2004) *Chem. Rev.* **104,** 403–418
30. Tsai, A.-L. (1994) *FEBS Lett.* **341,** 141–145
31. Traylor, T. G., and Sharma, V. S. (1992) *Biochemistry* **31,** 2847–2849
32. Boon, E. M., Davis, J. H., Tran, R., Karow, D. S., Huang, S. H., Pan, D., Miazgowicz, M. M., Mathies, R. A., and Marletta, M. A. (2006) *J. Biol. Chem.* **281,** 21892–21902
33. Draghi, F., Miele, A. E., Travaglini-Allocatelli, C., Vallone, B., Brunori, M., Gibson, Q. H., and Olson, J. S. (2002) *J. Biol. Chem.* **277,** 7509–7519
34. Pesce, A., Dewilde, S., Kiger, L., Milani, M., Ascenzi, P., Marden, M. C., Van Hauwaert, M. L., Vanfleteren, J., Moens, L., and Bolognesi, M. (2001) *J. Mol. Biol.* **309,** 1153–1164
35. Pesce, A., Nardini, M., Ascenzi, P., Geuens, E., Dewilde, S., Moens, L., Bolognesi, M., Riggs, A. F., Hale, A., Deng, P., Nienhaus, G. U., Olson, J. S., and Nienhaus, K. (2004) *J. Biol. Chem.* **279,** 33662–33672
36. Stasch, J. P., Becker, E. M., Alonso-Alija, C., Apeler, H., Dembowsky, K., Feurer, A., Gerzer, R., Minuth, T., Perzborn, E., Pleiss, U., Schroder, H., Schroeder, W., Stahl, E., Steinke, W., Straub, A., and Schramm, M. (2001) *Nature* **410,** 212–215
37. Hoenicka, M., Becker, E. M., Apeler, H., Sirichoke, T., Schroder, H., Gerzer, R., and Stasch, J. P. (1999) *J. Mol. Med.* **77,** 14–23
38. Friebe, A., Schultz, G., and Koesling, D. (1996) *EMBO J.* **15,** 6863–6868
39. Cary, S. P., Winger, J. A., Derbyshire, E. R., and Marletta, M. A. (2006) *Trends Biochem. Sci.* **31,** 231–239
40. Kharitonov, V. G., Sharma, V. S., Magde, D., and Koesling, D. (1997) *Biochemistry* **36,** 6814–6818
41. Kharitonov, V. G., Russwurm, M., Magde, D., Sharma, V. S., and Koesling, D. (1997) *Biochem. Biophys. Res. Commun.* **239,** 284–286
42. Rose, E. J., and Hoffman, B. M. (1983) *J. Am. Chem. Soc.* **105,** 2866–2873
43. Momenteau, M., and Reed, C. A. (1994) *Chem. Rev.* **94,** 659–698